

Inverse Z-spectrum analysis for MT- and spillover-corrected and T₁-compensated steady-state pulsed CEST-MRI – application to pH-weighted MRI of acute stroke

Moritz Zaiss¹, Junzhong Xu^{2,3}, Steffen Goerke¹, Imad S. Khan⁴, Robert J. Singer⁴, John C. Gore^{2,3,5}, Daniel F. Gochberg^{2,3,6}, Peter Bachert¹

¹Department of Medical Physics in Radiology, Deutsches Krebsforschungszentrum (DKFZ, German Cancer Research Center), Heidelberg, Germany

² Institute of Imaging Science, Vanderbilt University, Nashville, TN 37232, USA

³ Department of Radiology and Radiological Sciences, Vanderbilt University, Nashville, TN 37232, USA

⁴ Department of Neurological Surgery, Vanderbilt University, Nashville, TN 37232, USA

⁵ Department of Biomedical Engineering, Vanderbilt University, Nashville, TN 37232, USA

⁶ Department of Physics and Astronomy, Vanderbilt University, Nashville, TN 37232, USA

Keywords: CEST, MT, spillover, spin-lock, creatine, stroke, pH-weighted imaging

Word count: 6076

Running Head:

Simple spillover corrected and T₁ compensated CEST-MRI

Department of Medical Physics in Radiology,
Deutsches Krebsforschungszentrum (DKFZ),
Im Neuenheimer Feld 280, D–69120 Heidelberg, Germany

*Corresponding author:

.....

German Cancer Research Center (DKFZ)
Department of Medical Physics in Radiology
Im Neuenheimer Feld 280
D–69120 Heidelberg
Germany

List of Abbreviations

AREX	apparent exchange dependent relaxation
APT	amide proton transfer
CEST	chemical exchange saturation transfer
CERT	chemical exchange rotation transfer
CNR	contrast-to-noise ratio
cw	continuous wave
DC	duty cycle
EPI	echo planar imaging
FA	flip angle
gagCEST	glycosaminoglycan CEST
GRE	gradient echo
lab	label scan
M_0	thermal equilibrium magnetization
MT	magnetization transfer
MTR	magnetization transfer ratio
MTR_{asym}	magnetization transfer ratio asymmetry
MTR_{normref}	magnetization transfer ratio normalized by reference scan
MTR_{pcm}	magnetization transfer ratio of probabilistic combined model
MTR_{Rex}	spillover corrected magnetization transfer ratio yielding R_{ex}
$M_{z,\text{sat}}$	z-magnetization after saturation
NOE	nuclear Overhauser effect
ref	reference scan
R_{eff}	effective water relaxation in the rotating frame
R_{ex}	exchange dependent relaxation in the rotating frame
rf	radiofrequency
ST	saturation transfer
TSE	turbo spin echo
WASSR	water saturation shift referencing
Z	normalized z-magnetization after saturation ($M_0/M_{z,\text{sat}}$)
Z_{lab}	Z-value of label scan
Z_{ref}	Z-value of reference scan

Abstract

Endogenous chemical exchange saturation transfer (CEST) effects are always diluted by competing effects such as direct water proton saturation (spillover) and macromolecular magnetization transfer (MT). This leads to unwanted T_2 and MT signal contributions that lessen the CEST signal specificity to the underlying biochemical exchange processes. A spillover correction is of special interest for clinical static field strengths and protons resonating near the water peak. This is the case for all endogenous CEST agents, such as amide proton transfer, $-OH$ -CEST of glycosaminoglycans, glucose or *myo*-inositol, and amine exchange of creatine or glutamate. All CEST effects appear also to be scaled by the T_1 relaxation time of water, as they are mediated by the water pool. This forms the motivation for simple and novel metrics that correct the CEST signal.

Based on eigenspace theory we propose novel magnetization transfer ratio (MTR_{Rex}), based on the inverse Z-spectrum, which eliminates spillover and macromolecular MT effects. This metric can be simply related to R_{ex} , the exchange-dependent relaxation rate in the rotating frame, and k_a , the inherent exchange rate. Furthermore, it can be scaled by the duty-cycle, allowing for simple translation to clinical protocols. For verification, the amine proton exchange of creatine in solutions

with different agar concentration was studied experimentally at clinical field strength of 3 T, where spillover effects are tremendous. We demonstrate that spillover can be properly corrected and also quantitative evaluation of pH and creatine concentration is possible. This proves that MTR_{Rex} is a quantitative and biophysically specific CEST-MRI metric. Applied to acute stroke induced in rat brain, the corrected CEST signal shows significantly higher contrast between stroke area and normal tissue as well as less B_1 dependency compared to conventional approaches.

Introduction

CEST exploits chemical exchange of labile protons either in metabolites or contrast agents to transfer labeled magnetization to the water pool (1–3). The CEST signal is obtained by water signal acquisition after selective rf irradiation at the resonance frequency of an exchanging proton pool. Together with a reference scan the water signal decrease due to saturation transfer can be determined. This leads to increased sensitivity mediated by the accumulation of the labeled state in the water pool. As the labeling of the exchanging protons can be done selectively by radio frequency (rf) irradiation at the specific chemical shift, CEST yields biochemical information of living tissue. Several CEST-MRI approaches were reported that enable monitoring cellular metabolites *in vivo*: amide–proton–CEST (4), creatine–CEST (5,6), glutamate–CEST (7), glycosaminoglycan–CEST (8–10), glucose–CEST (11) and also many paramagnetic exogenous agents (3). Some exchange processes are distinctly pH-sensitive and allow pH-weighted MRI (4,12–14). This makes CEST imaging interesting for characterizing of ischemic lesions as they occur in stroke where a drop of the amide proton transfer peak is reported (15–17).

However, the rf irradiation used for labeling also excites nearby resonances. Especially for clinical static field strengths and endogenous amide, amine, and hydroxyl protons, CEST pools resonate close to the water peak with the consequence that direct saturation of the water protons surpasses the CEST effect. The impact of direct water saturation on the CEST pool resonance is called “spillover”. Moreover, magnetization transfer (MT) effects owing to broad macromolecular resonances are apparent, even far away from the water peak and overlay the CEST effect. Both spillover and MT effects grow with increasing rf irradiation amplitude B_1 (18,19). Likewise, solute labeling (and hence the possible maximum CEST effect) also increases with B_1 (20). Thus, CEST sequences are often optimized by variation of B_1 to yield maximum contrast (7,10,11), but the signal at optimal B_1 is highly sensitive to spillover (21) and correction is especially required in this optimal case. Finally, as mediated by the water pool, the water T_1 scales the strength of the whole effect.

To assess the physiological relevance of any MR imaging contrast, artifacts and sources of non-specific contrast must be identified, explained and eliminated as far as possible. This problem is an active area of research in the CEST community and several approaches were suggested to correct for the described effect: simple asymmetry analysis (4), Lorentzian line fits (22), or Lorentzian differences (23,24), or more sophisticated isolation approaches such as double frequency irradiation (25,26) and chemical exchange rotation transfer (27,28). However, even CEST signals isolated from concomitant effects, such as T_2 or MT, can still be diluted by them (19,20). Thus, isolation often isolates an already diluted effect by spillover and MT does generally not imply spillover and MT correction: these are different issues.

Therefore, we propose a new evaluation method which is simply applicable to Z-spectrum data and able to both isolate and correct the effects on the CEST signal from spillover, MT and T_1 . The approach uses the inverse metric of the Z-spectrum ($1/Z$) to obtain spillover- and MT-corrected CEST-MRI data. Our approach is based on the equivalence of spinlock (SL) and CEST experiments (29). By employing a solution of Santyr *et al.* (30) proposed for pulsed SL, we extend this equivalence to pulsed CEST which is required in applications to clinical MR scanners. As a proof-of-principle we present data from creatine–agar model solutions, but expect that this approach is generally applicable to all types of CEST experiments driven to steady-state. We also demonstrate that the inverse metric $1/Z$ is useful not only for corrections, but also for quantitative CEST-MRI. Finally, we apply the correction to amide proton transfer (APT) imaging in acute stroke, where a pure exchange-weighted contrast might help in the characterization of lesions.

Theory

The Z-spectrum and useful magnetization transfer ratios for cw-CEST

We first compile results of cw theory (31,32) for two exchanging pools, the abundant pool a (water pool) with thermal magnetization M_{0a} and the rare pool b (CEST pool) with thermal magnetization M_{0b} . For most metabolite/water systems an asymmetric population given by the proton fraction $f_b = M_{0b}/M_{0a} < 1\%$ can be assumed. Both pools undergo longitudinal and transverse relaxation with rates R_{1a} , R_{2a} , R_{2b} . The longitudinal relaxation of pool b, R_{1b} , is assumed to be small compared to the exchange rate and will be neglected in the following (32). The pools are coupled by the exchange rate k_b and the back exchange rate $k_a = f_b \cdot k_b$. The rf irradiation amplitude ($\omega_1 = \gamma B_1$) and offset frequency from water ($\Delta\omega$) define the off-resonant saturation which leads to an effective field vector $\omega_{\text{eff}} = (\omega_1, 0, \Delta\omega)$ tilted by the angle $\theta = \tan^{-1}(\omega_1/\Delta\omega)$ off the z axis. (18, 22). The steady-state magnetization after saturation, M_{sat} , normalized by the thermal magnetization M_{0a} , was named Z-value by Woessner *et al.* (33). The Z-spectrum or $Z(\Delta\omega)$ is given by (32)

$$Z(\Delta\omega) = \frac{M_{\text{sat}}(\Delta\omega)}{M_{0a}} = \cos^2 \theta \frac{R_{1a}}{R_{1\rho}} \quad (1)$$

where $R_{1\rho}$ is the longitudinal relaxation rate of the water pool in the rotating frame

$$R_{1\rho} = R_{\text{eff}} + R_{\text{ex}} \quad (2)$$

R_{ex} is the exchange-dependent relaxation in the rotating frame; R_{eff} corresponds to $R_{1\rho}$ of the water pool when there is no exchange and reads

$$R_{\text{eff}} = R_{1a} \cos^2 \theta + R_{2a} \sin^2 \theta \quad (3)$$

This rate arises from the relaxation due to direct water saturation and is the origin of the spillover effect. If also a symmetric MT is apparent, R_{eff} can be extended (32,34) by an exchange relaxation for MT to $R_{\text{eff}} = R_{1a} \cos^2 \theta + R_{2a} \cos^2 \theta + R_{\text{ex}}^{\text{MT}}$. ~~As we remove R_{eff} in the following, the exact knowledge of R_{2a} or $R_{\text{ex}}^{\text{MT}}$ is not important, so long as R_{eff} stays symmetric in $\Delta\omega$.~~ As we remove R_{eff} in the following, the exact knowledge of R_{2a} or $R_{\text{ex}}^{\text{MT}}$ is not important, as long as we have a reference value with the same R_{eff} . In agar phantoms, R_{eff} stays symmetric in $\Delta\omega$ and the opposite frequency can be used. *In vivo*, the baseline can be estimated by a three-point method (eq. (21)).

The exchange weighting in CEST-MRI is induced by the rate R_{ex} . Hence an appropriate evaluation method must provide direct access to R_{ex} . R_{ex} can be approximated by (32)

$$R_{\text{ex}}(\Delta\omega_b) = k_b f_b \cdot \alpha \frac{\Gamma^2/4}{\Gamma^2/4 + \Delta\omega_b^2} \quad (4)$$

where $\Delta\omega_b$ is the frequency offset with respect to the CEST pool b. The labeling efficiency can be approximated by (32)

$$\alpha = \frac{\omega_1^2}{\omega_1^2 + k_b(k_b + R_{2b})} \quad (5)$$

R_{ex} is a Lorentzian function of $\Delta\omega_b$ with its maximum at $\Delta\omega_b = 0$ and linewidth

$$\Gamma = 2\sqrt{\frac{k_b + R_{2b}}{k_b} \omega_1^2 + (k_b + R_{2b})^2} \quad (6)$$

A useful quantity is the magnetization transfer ratio asymmetry (MTR_{asym}), which attempts to isolate the contributions of CEST effects to the Z-spectra by using a reference scan without CEST effects, which can be the scan at opposite frequency or the fit of direct water saturation (23,24).

For agar phantoms, we use the opposite frequency signal as a reference. To abbreviate the following relations we define the label scan around the resonance of pool b as $Z_{\text{lab}} = Z(+\Delta\omega)$ and the reference scan at the opposite frequency with respect to water as $Z_{\text{ref}} = Z(-\Delta\omega)$. For $Z_{\text{ref}} = Z(-\Delta\omega)$, the effective relaxation $R_{\text{eff}}(-\Delta\omega)$ is unchanged, i.e. $R_{\text{eff}}(-\Delta\omega) = R_{\text{eff}}(\Delta\omega)$. Hence, R_{ex} is only important for the labeling scan and R_{ex} can be neglected for the opposite frequency. Thus the opposite frequency can be used as a reference scan $Z_{\text{ref}} = Z(-\Delta\omega)$. (This reasoning assumes (1) that R_{eff} is symmetric and that no MT asymmetry or additional exchanging pools at $-\Delta\omega$ are present; and (2) that the width Γ of $R_{\text{ex}}(\Delta\omega_b)$ is smaller than the chemical shift ($\Gamma < \delta_b$) of the corresponding pool.

For continuous wave (cw) steady-state it was shown previously (32) that there are different MTR normalizations possible. The most common is the subtraction of Z-values of label and reference scan giving the asymmetry of the Z-spectrum:

$$MTR_{\text{asym}} = Z_{\text{ref}} - Z_{\text{lab}} = \cos^2 \theta \frac{R_{\text{ex}} R_{1a}}{R_{\text{eff}} (R_{\text{eff}} + R_{\text{ex}})} \quad (7)$$

A reported spillover-corrected evaluation proposed by Liu *et al.* (35,36) normalizes with the reference value

$$MTR_{\text{normref}} = \frac{Z_{\text{ref}} - Z_{\text{lab}}}{Z_{\text{ref}}} = \frac{R_{\text{ex}}}{R_{\text{eff}} + R_{\text{ex}}} \quad (8)$$

A probabilistic combined model (pcm) for Z-spectra able to separate CEST from spillover and MT of Zaiss *et al.* (22) can also be written as a magnetization transfer ratio:

$$MTR_{\text{pcm}} = \frac{Z_{\text{ref}} - Z_{\text{lab}}}{Z_{\text{ref}} - Z_{\text{lab}} + Z_{\text{lab}} Z_{\text{ref}}} = \frac{R_{\text{ex}}}{\cos^2 \theta \cdot R_{1a} + R_{\text{ex}}} \quad (9)$$

This evaluation easily leads to the ideal proton transfer rate $\text{PTR} = k_a / (k_a + R_{1a})$ (1,37). However, the straightforward way to separate for R_{ex} is by the use of the subtraction of the inverse Z-values:

$$MTR_{R_{\text{ex}}} = \frac{1}{Z_{\text{lab}}} - \frac{1}{Z_{\text{ref}}} = \frac{R_{\text{ex}}}{\cos^2 \theta \cdot R_{1a}} \quad (10)$$

While MTR_{asym} contains a quadratic term of R_{eff} and MTR_{normref} still a linear term of R_{eff} in the denominator, note that MTR_{pcm} and $MTR_{R_{\text{ex}}}$ are free of R_{eff} terms and therefore particularly free of R_{2a} and symmetric MT contributions.

The Z-spectrum and useful magnetization transfer ratios for pulsed-CEST

The assumption of R_{1p} decay during the pulse (pulse duration t_p) and R_{1a} recovery during rf off (interpulse delay time t_d) leads to the following formula for the steady-state in a pulsed SL experiment (30):

$$Z_{\text{pulsed}}^{\text{ss}}(\Delta\omega) = \frac{(1 - e^{-R_{1a} \cdot t_d}) - \frac{R_{1a} \cdot \cos \theta}{R_{1\rho}(\Delta\omega)} (1 - e^{R_{1\rho}(\Delta\omega) \cdot t_p})}{e^{R_{1\rho}(\Delta\omega) \cdot t_p} - e^{-R_{1a} \cdot t_d}} \quad (11)$$

This is the result of Santyr *et al.* (30) in our notation. Assuming small arguments of the exponential functions we employ $\exp(x) \cong 1+x$ and obtain – with duty-cycle $DC = t_p/(t_p+t_d)$ – an expression for the normalized steady-state magnetization Z_{SS} which is similar to the result for the cw case

$$Z_{\text{pulsed}}^{\text{ss}}(\Delta\omega) \approx \frac{R_{1a}(1 - DC + \cos \theta \cdot DC)}{R_{1\rho}^{\text{pulsed}}(\Delta\omega)} \quad (12)$$

where

$$R_{1\rho}^{\text{pulsed}}(\Delta\omega) = R_{1\rho}(\Delta\omega) \cdot DC + R_{1a} \cdot (1 - DC) \quad (13)$$

Assuming $\cos \theta = 1$ and employing eqs. (12) and (13) for the magnetization transfer rates MTR_{pcm} (eq. (9)) and $MTR_{\text{Re}x}$ (eq. (10)) leads to the pulsed MTRs:

$$MTR_{\text{pcm}} = \frac{R_{\text{ex}} \cdot DC}{R_{1a} + R_{\text{ex}} \cdot DC} \quad (14)$$

$$MTR_{\text{Re}x} = \frac{R_{\text{ex}} \cdot DC}{R_{1a}} \quad (15)$$

Therefore, the pulsed MTRs are only altered by the duty-cycle as a prefactor of R_{ex} against the cw case (cmp. Eqs. (9) and (10)). Thus, this spillover and MT correction is likewise applicable to pulsed CEST.

Quantitative Parameter Determination

Equation 10 (with expected parameter dependencies as described in eq. (15)) provides a robust measure for qualitative contrast that avoids the effects from direct water saturation and exchange from symmetric macromolecular MT effects and is hence superior to the current standard MTR_{asym} . However, ideally we would like a metric that quantitatively reports on a fundamental sample parameter. To extend this spillover correction method to a quantification method we define the apparent exchange-dependent relaxation AREX

$$\text{AREX} = MTR_{\text{Re}x} \frac{R_{1a}}{DC} = R_{\text{ex}} \quad (16)$$

AREX should yield R_{ex} which is given by equation (4) and the labeling efficiency α (eq. (5)). We can assume the maximum labeling efficiency ($\alpha \cong 1$) as long as the conditions $k_b \ll \omega_1$ and $R_2 \ll \omega_1$ hold (eq. (5)). In this full-saturation limit, when applying irradiation at the b-pool resonance, $R_{\text{ex}} = k_b \cdot f_b = k_a$ (eqs. (7) and (12)) and hence,

$$\text{AREX} = k_a \quad (17)$$

Instead of modeling a pulse train by an average B_1 power we now obtain a DC weighting of an average R_{ex} during the pulse. The implicit assumption that the average $R_{1\rho}$ during the pulse equals the cw relaxation rate is discussed below.

In summary, two conditions must be valid for $AREX = k_a$: Firstly, the full-saturation limit $\omega_1 \gg k_b$, and secondly, R_2 and the peak width (eq. (6)) must be smaller than the chemical shift difference to water ($\Gamma < \delta_b$). Considering amide protons of proteins at $B_0 = 3T$, the CEST pool parameters are $k_b \approx 30 \text{ s}^{-1}$ and $\delta_b = 3.5 \text{ ppm}$ ($=447 \cdot 2\pi \text{ s}^{-1}$) (1,38). As a model for amide exchange we employ amine protons of creatine at lower pH (6.2–6.6) to obtain a comparable exchange rate ($k_b \approx 30 - 60 \text{ s}^{-1}$) (19). The smaller chemical shift $\delta_b = 1.9 \text{ ppm}$ ($=242 \cdot 2\pi \text{ s}^{-1}$) challenges our method for spillover correction and is therefore a crucial test. For $1 \mu\text{T} < B_1 < 5 \mu\text{T}$ both conditions are well fulfilled for creatine amine and amide protons:

$$k_b = 50 \text{ s}^{-1} \ll \omega_1 = \frac{B_1}{\mu\text{T}} \cdot 42.6 \cdot 2\pi \text{ s}^{-1} \cong \frac{\Gamma}{2} < \frac{\delta_b}{2} = 121 \cdot 2\pi \text{ s}^{-1}.$$

In general, if peaks are broad and other pools c are involved the reference scan is also contaminated by non-zero exchange-dependent relaxation terms $R_{ex,ref} = R_{ex}(-\Delta\omega)$ in addition to the on-resonant term $R_{ex,lab} = R_{ex}(\Delta\omega)$. Thus, AREX yields

$$AREX = R_{ex,lab}^b - R_{ex,ref}^b + R_{ex,lab}^c - R_{ex,ref}^c \quad (18)$$

instead of $R_{ex,lab}$. Although affected by the pool c and therefore being not selective anymore, the resulting MTR_{ex} is still free from symmetric spillover effects and hence an apparent R_{ex} (AREX) which is still a pure exchange-dependent parameter.

pH mapping

Under assumption of full saturation, AREX is given by $k_b f_b$. Therefore, AREX of APT can be used to calculate the exchange rate by the formula previously derived by Sun *et al.* (39):

$$\text{pH}(in vivo) = 6.4 + \log_{10}\left(\frac{AREX}{f_b \cdot 5.57}\right) \quad (19)$$

For APT $f_b = 1:867$ was reported (39). For amine exchange of creatine the $k(\text{pH})$ dependency was given by Goerke *et al.* (40). It can be rearranged yielding the absolute pH employing an AREX map:

$$\text{pH}(19^\circ\text{C}) = \log_{10}\left(\frac{AREX}{f_b \cdot 1.4615}\right) \quad (20)$$

A flow chart of how the theory and evaluation methods are applied to the raw data is given in Figure 1.

Methods

The proposed spillover correction based on the inverse metric was tested in CEST experiments with creatine model solutions at $B_0 = 3 \text{ T}$ as well as *in vivo* rat measurements at 9.4T.

Phantoms

Eleven phantoms containing phosphorus-based sodium-potassium buffer at different pH values were measured. Their marks are shown in Figure 2 and their properties are listed in Table 1. Creatine-monohydrate (Sigma-Aldrich, Steinheim, Germany) of 55.5 mM concentration was added to each 50-ml tube. Two tubes had different creatine concentrations #F1: $(2/3) \times 55.5 \text{ mM}$ and #F2: $(1/3) \times 55.5 \text{ mM}$.

To vary the conditions for spillover and MT, 0.2% to 1% agar was added to a 55.5-mM creatine solution at pH = 6.38 (#A1 – #A5, “solidified phantoms”). The pH value did not change during the heating process and addition of agar. Phantom #0 contained no agar as well as #PH1–PH3 which are controls with different pH of 6.2, 6.3, and 6.6, respectively.

Phantom parameters were estimated for a two-pool model by a full numerical fit of Z-spectra obtained for different rf amplitudes B_1 (numerical QUESP (41)).

***In vitro* MRI experiments**

Phantom imaging was performed on a 3-T whole-body MR scanner (Magnetom TIM-TRIO; Siemens, Erlangen, Germany). Z-spectra were obtained after saturation by a train of 80 Gaussian-shaped pulses with duration $t_p = 100$ ms of each pulse and interpulse delay $t_d = 100$ ms (DC = 50%) at $B_1 = \text{flip angle}/(\gamma t_p) = 0.2\text{--}2$ μT followed by single-shot TSE imaging (FOV (220 mm)², matrix 192×192, in-plane resolution 1.1×1.1×4 mm³). Z-spectra were B_0 -corrected employing a WASSR map (42). After B_0 correction the MTRs according to equations (7), (8), (9), and (10) were calculated pixel-by-pixel and by ROI evaluation employing the opposite frequency as reference scan Z_{ref} . MTR_{Rex} was compared to analytical R_{ex} and k_a values determined by the numerical fit. Fitting of Z-spectra was performed by stepwise matrix solution (33) of the 2-pool Bloch-McConnell equations.

T_1 -weighted MR images were acquired by a saturation recovery GRE (TE = 4 ms, TR = 8 ms, 4 shots, 4 averages, FOV (220 mm)², matrix 256×256, in-plane resolution 0.9×0.9×4 mm³, flip angle = 8°). Altogether 21 contrasts at different recovery times between 50 ms and 5 s were fitted to obtain T_1 maps.

T_2 -weighted MR images were acquired by a spinecho sequence with 32 echo delays (TE = 11 ms to 352 ms, TR = 6 s, FOV (220 mm)², matrix 192×192, in-plane resolution 1.1×1.1×4 mm³, flip angle = 180°). A pixel-by-pixel logarithmic fit was applied to obtain T_2 maps.

Animal preparation

All animal-related procedures were approved by the Institutional Animal Care and Use Committee at the Vanderbilt University. The middle cerebral artery occlusion model (MCAO) was adapted on Spontaneously Hypertensive male rats (Charles Rivers Laboratory) weighing between 275 and 300 g as previously described (43). Specifically, rats were anesthetized with isoflurane (3% for induction and 2% during surgery) via a vaporizer with O₂. A midline neck incision was made and the common, external and internal carotid arteries were identified on the right side and isolated from the surrounding structures. The proximal branches of the external carotid artery were ligated and an arteriotomy was made in the external carotid artery. A 0.37-mm diameter silicon-coated 4-0 nylon suture (Doccol Corporation, Redlands, CA) was introduced into the vessel and routed into the internal carotid artery. The suture was pushed into the internal carotid artery until a mild resistance was felt and the MCA was occluded (at a length of 18–20 mm) and the suture was left there. Body temperature was maintained with a heating pad during surgery. The wound was then closed and buprenorphine was administered for post-operative pain management.

***In vivo* MRI experiments**

Animal imaging was performed 48 hours after surgery on a 9.4-T horizontal MRI scanner (Varian, Palo Alto, CA, USA). Bite bar and head bar were used to secure the animal during imaging to reduce respiration-induced motion artifact. The rectal temperature was kept at 37°C using a warming-air feedback system. A single-shot echo planar imaging (EPI) was used for the acquisition and a triple-reference imaging scheme (44) was used to reduce EPI artifacts. Measurement parameters were: matrix size = 64, echo time = 28 ms. Pulse train parameters were $t_p = 12.5$ ms, $B_1 = 0.84$ μT , DC = 50%, flip angle = 180°, $n = 200$.

Evaluation

For the phantom preparation creatine was employed as CEST agent and agar was used to solidify several tubes, changing the properties of the water pool. The opposite frequency is a reasonable choice for the reference scan ($Z_{ref} = Z(-3.5\text{ppm})$) for the phantom study. However, in *in vivo* Z-spectra the opposite side is contaminated by MT and peaks owing to nuclear Overhauser effects (NOE). Therefore, for *in-vivo* APT signal, the three point method proposed by Jin et al. (45) was employed, in a pixel-by-pixel basis. Using the same Z_{ref} ,

$$Z_{ref}^* = \frac{Z(3.0\text{ppm}) + Z(4.2\text{ppm})}{2}; Z_{lab} = Z(3.5\text{ppm}) \quad (21)$$

we define the spillover- and MT-corrected parameter MTR_{Rex}

$$MTR_{Rex}^* = 1/Z_{lab} - 1/Z_{ref}^* \quad (22)$$

and, according to eq. (16), also the T_1 -relaxation-compensated parameter AREX*. To enhance sensitivity for ROI evaluations, the MTR values of 3.4 ppm, 3.5 ppm and 3.6 ppm were averaged by using a Z_{ref} from a linear interpolation of the points at 3 ppm and 4.2 ppm.

Results

The results section is divided in three parts. First, we present the outcome of Z-spectroscopy of the solidified phantoms and how the different metrics allow for spillover correction. Secondly, we show the quantitative metric AREX and how exchange rate and pH mapping can be obtained after compensation of effects of T_1 -relaxation. Thirdly, the metrics are applied to *in vivo* data of stroke in rat brain.

Spillover correction

Figure 3a shows distinct effects in the Z-spectrum upon addition of 1% agar (phantom #A5) in experiments at $B_0 = 3$ T. The corresponding asymmetry is strongly diluted compared to the creatine solution without agar (phantom #0) (MTR_{asym} , Figure 3b). Even in the case of full saturation of the CEST pool ($B_1 > 1$ μ T) we still observe a strong dependence of MTR_{asym} on B_1 in the solidified phantom. $MTR_{normref}$ (Figure 3c) provides an enhancement of the signal of the solidified phantom, but displays an underestimation of the CEST effect by about 30 % and a strong dependence on the amplitude B_1 of the saturating field. Both MTR_{pcm} and MTR_{Rex} give very similar values for solidified and non-solidified phantoms. This can be seen not only in the case of on-resonant irradiation on pool b, but also the shape of the CEST peak is coherent with the peak of the control measurement in the absence of agar. This proves the validity of our spillover correction for arbitrary frequency offsets. In the case of full saturation the dependence of MTR_{Rex} and MTR_{pcm} on B_1 is less than 15%, producing a small overestimation of the effect. Near the center of the water proton resonance at 0 ppm all MTRs show considerable deviations which are even larger for the inverse MTR_{pcm} and MTR_{Rex} . Errors increase tremendously which is discussed in detail below (Figure 10).

Images of MTR_{asym} and MTR_{Rex} at 1.83 ppm display the same relation: Spillover is uncritical for small B_1 , whereas for stronger B_1 spillover dilutes MTR_{asym} significantly. In contrast, MTR_{Rex} yields an homogeneous contrast up to $B_1 = 1.4$ μ T independent of the agar concentration (Figure 4). Figure 4 demonstrates the importance of spillover correction since MTR_{asym} causes misinterpretation of diluted signals as changes in pH or concentration. At $B_1 = 2$ μ T the agar tubes #A2 and #A3 show a very similar contrast as the tube #F2 in presence of one third of the creatine concentration. For exceedingly high B_1 , the contrast-to-noise ratio is insufficient and MTR_{Rex} cannot completely

reconstruct the ideal signal from the residual signal. MTR_{Rex} also enhances the signals from the tubes without agar: different pH and different concentration can therefore even better be distinguished after correction.

Figure 5 displays MTR as a function of B_1 . Using MTR_{Rex} or MTR_{pcm} the plateau of the full-saturation limit is reached, while MTR_{asym} and MTR_{normref} show the known decrease of the CEST effect due to spillover dilution induced by MT, T_2 relaxation, and B_1 . Thus in the full-saturation limit a spillover correction is also a first-order B_1 correction.

Quantification

The numerical Bloch-McConnell fit of ROI-averaged Z-spectra for different B_1 yields the characterization of the phantom parameters listed in Table 1. The values for exchange rates k_b agree well with WEX data measured by Goerke *et al.* (40). The relative concentrations f_b are in good agreement with the prepared creatine concentration if the number of exchanging protons per molecule is 4. R_{2b} values are quite constant with a value of ca. 50 s^{-1} , which is comparable to the exchange rate.

MTR_{Rex} and MTR_{pcm} were calculated using B_1 , DC, k_b , f_b , R_{1a} , R_{2b} , and the theoretical rate R_{ex} (eq. (4)). Actually, the pulsed approach of Santyr *et al.* (30) is known to deviate especially for slow exchange rates (46). Roelloeffs *et al.* (46) showed that a biexponential decay during the break has to be modeled to properly extend the model of Santyr. For spillover and MT correction we think this is not important as the deviation is still only exchange dependent, for quantification this may have an influence. Nevertheless, the comparison of MTR_{Rex} calculated from fit results with MTR_{Rex} obtained from data (Figure 5) shows that corrected curves can still be interpreted by the analytical solution for MTR_{Rex} (eq. (10)(15)) based on Santyr's model. We think that because we used 100ms Gaussian pulses - which end with a low power - the equilibrium between pool a and pool b is not too much changed directly after the pulse, making the biexponential decay less important. However, this should be studied in detail and may limit our approach for pulsed CEST of slow exchanging systems saturated with different pulse shapes. However, with our pulse parameters the step from spillover-corrected MTR_{Rex} to a reliable quantification of the back exchange rate k_a is straightforward by employing eq. (17) (Figure 6). AREX is therefore proportional to the concentration f_b and the exchange rate k_b . It varies between phantoms #F1, #F2 and #0 and also between phantoms #0, #PH1, #PH2, and #PH3. AREX yields homogeneous contrast in phantoms #0, #A1-A5. However, a small overestimation of k_a in the agar phantoms compared to the control (#0) is observed.

Using the exchange rate of creatine protons, $k_b(\text{pH} = 6.38, T = 19^\circ\text{C}) = 35 \text{ s}^{-1}$, measured in WEX experiments (40), a map of the relative proton fraction f_b can be obtained which is valid for the given pH and is in agreement with fit results. Together with the prepared creatine concentration (55.5 mM) this approach yields the number of labile protons per creatine molecule, $N = f_b \times [2\text{H}_2\text{O}]/[\text{Cr}]$. For $\text{pH} \leq 6.4$, N is most probably 4, in conformity with the zwitterionic structure of creatine (Figure 2b) and the pK_a value of the creatine amine groups $\text{pK}_a = 6.6$ at $T = 37^\circ\text{C}$ (5). For the phantom at $\text{pH}=6.6$ the proton number might be smaller. Assuming 4 exchanging amine protons for creatine the value of f_b can be derived for any creatine concentration. Together with $\text{AREX} = k_a$ we obtain a k_b -map. Finally, using the dependence of the creatine amine exchange rate k_b on pH found by Goerke *et al.* (40), a map of absolute pH values can be calculated. The resulting data is in good agreement with pH values prepared in the phantoms (Figure 6). This proves that spillover, MT, and T_1 -relaxation compensation worked well for the creatine-agar phantoms.

Application *in vivo*

Having demonstrated the validity of the introduced corrections, the formalism can be applied to *in vivo* data. In a stroke lesion of rat brain we expect a drop of APT due to pH drop, which is clearly

visible in Figure 7. The Z-spectrum at 3.5 ppm is contaminated by direct saturation and MT effects (Figure 7d,g), therefore the baseline estimation of Jin *et al.* (45) was employed as a reference. After correction of spillover by MTR_{Rex} the contrast to noise ratio (CNR) between normal and lesion tissue increases from $CNR=1.17$ to $CNR=1.44$ (values correspond to ROIs in Figure 8). Also the T_1 -map (Figure 7e) shows a difference between lesion and healthy tissue (Figure 7b). This can be corrected by the AREX evaluation showing an even higher $CNR=1.62$ between normal and pathologic tissue (Figure 7c). Please note that delay time and rotation transfer effects were taken into account by using $DC=1$ to calculate AREX. Finally, employing equation (19) and the reported proton fraction $f_b = 0.115\%$ a absolute pH map can be calculated from AREX. It shows pH values between 7 and 7.2 in normal tissue and a drop to around 6.5 within the lesion (Figure 7f).

A further check of the spillover correction is possible by investigating the behavior for increasing B_1 which was shown for phantoms in Figure 4. A similar signature in the MTRs as a function of B_1 was observed after spillover correction of ROI averaged data (Figure 8b, c): For low B_1 APT*, MTR_{Rex} *, and AREX* show an increase with B_1 . After reaching a maximum at 1.6 μT signals drop again. However, the decrease for the spillover-corrected methods is less significant and a kind of plateau is reached. Again, the APT contrast after spillover correction is shown to be less B_1 -dependent. Important to note is the increase of contrast between tissue in the lesion and normal tissue. For AREX the contrast difference is much larger than the standard deviation. Therefore, AREX leads to a more pure, but also larger contrast.

Discussion

In this study we showed that a magnetization transfer ratio employing the inverse metric of the Z-spectrum enables removal of spillover and MT effects from CEST signals.

As depicted in Figure 1 only simple mathematical operations are needed to get a spillover-corrected signal from raw Z-spectra data. Previous studies on spillover by Sun *et al.* (19,20,47) treated the spillover effect by introducing a spillover coefficient σ of the ideal magnetization transfer rate, i.e. $MTR_{\text{real}} = (1-\sigma) \cdot \alpha \cdot MTR_{\text{ideal}}$ (α is the labeling efficiency, eq. (7)). In contrast to this approach, we observed that spillover dilution can be better explained by the inverse addition of contributing effects. Spillover dilution of a CEST effect induced by “parallel” saturation of water resembles the “dilution” of a resistor R_b by a parallel circuit to another resistor R_a . If the diluted resistance R_{a+b} and the resistance of R_a are known, one obtains $1/R_b = (1/R_{a+b}) - (1/R_a)$.

The reason why superposition and not inverse superposition of effects in the Z-spectrum were also successful in other treatments results originates from the approximation $Z = 1/(1+x) \approx (1-x)$ valid for $R_{\text{eff}} \approx R_{1a}$ and small $x \approx R_{\text{ex}}/R_{1a}$. This is also the principal reason why superpositions of Lorentzians can be fitted to steady-state-pulsed CEST spectra. According to our results a superposition of reciprocal Lorentzians should be more suitable. The observation that $1/Z$ yields basically an $R_{1\rho}$ spectrum (eq. (1)) further supports the importance of the inverse Z-spectrum. $R_{1\rho}$, known from spinlock experiments, has, as a relaxation rate, the property of being a superposition of the apparent exchange-dependent relaxation effects (eq. (2) (48)).

Some degree of dilution was identified as spillover effect by Sun *et al.* (19,20,47). In our approach this contribution is regarded as a loss in labeling efficiency. The latter can be defined more generally as $\alpha = R_{\text{ex}}/k_a$ yielding (29):

$$\alpha = \frac{(\omega_b - \omega_a)^2}{\omega_1^2 + \Delta\omega^2} \underbrace{k_b + R_{2b}}_* \frac{\omega_1^2}{\omega_1^2 + k_b (k_b + R_{2b})} \quad (23)$$

A comparison of eq. (23) with α of eq. (5), which is similar to the α given in of Ref. (37), reveals an additional factor (*) in eq. (23), which decreases with increasing B_1 . This factor is maximal at $\Delta\omega = 0$ and can be interpreted as on-resonance effects induced by the exchange. Those effects are employed in on-resonant spinlock experiments. The loss of labeling is attributed to an interference of off-resonant and on-resonant features of R_{ex} . Hence, labeling efficiency is an useful parameter which was extended by the eigenspace approach (29), whereas a spillover coefficient is not appropriate to the inverse metric.

Other than the spillover correction employed by Sun *et al.* (19) and the “isolation” of R_{ex} from $R_{1\rho}$ ($R_{ex} = R_{1\rho} - R_{eff}$) proposed by Jin *et al.* (14), which both use additional T_2 - and B_1 -mapping, our approach employs only the intrinsic metric to correct spillover. This is advantageous because it reduces scanning time and post-processing efforts. The intrinsic structure was employed in a similar manner in the fit model of Ref. (22) which is the origin of MTR_{pcm} (eq. (5)).

It is important to note that isolation and correction of effects are different operations. Whereas the former approaches like MTR_{asym} , isolate signals from specific effects, these isolated effects can still be diluted (Figure 3). Therefore, removing the information about parallel effects must be considered carefully, since other contributions may become invisible, but can still be effective as dilutions.

The approach of Liu *et al.* (35) (eq. (8)) afforded a partial spillover correction which could be explained by the reduction of the quadratic term of R_{eff} in MTR_{asym} to a linear one. Their normalization is considered to be appropriate for glutamate CEST imaging (7,49) and gagCEST (50). In particular, these two applications can also benefit from the improvement of the MTR_{Rex} evaluation.

Next we discuss our quantitative approach. To the best of our knowledge, there are two different approaches to model the pulsed-CEST case. On the one hand, using cw theory with an equivalent cw power (12,51) verified to be valid for slow exchange rates by Tee *et al.* (52). On the other hand, the approach of Santyr *et al.* (30) for spinlock which should also be valid for CEST by relying on the equivalence of spinlock and CEST (29). Santyr's spinlock solution takes into account different relaxation during and between the pulses. However, Santyr *et al.* assume solely monoexponential decay in the interpulse delay which cannot explain the modulations as a function of the flip angle observed by chemical exchange rotation transfer (CERT) (28) or the dependency on delay time (53). However, for long pulses, as employed in this study, our results suggest that Santyr's approach is also valid for pulsed CEST. We observe no perfect match of Santyr's theory and the corrected data, what we attribute to the invalid assumption of monoexponential dynamics in the interpulse delay and the assumption of full saturation ($R_{ex} = k_a$) during the Gaussian pulse. The R_{ex} obtained by AREX is therefore an effective parameter which incorporates the dependence on pulse shape as well as processes occurring between the pulses.

The inverse metric is valid only for pulsed CEST/SL if $R_{1\rho} \cdot t_p \ll 1$ (assumption of eq. (12)) which is not the case for large R_2 and θ or t_p . This could explain why the agar phantoms show slightly different MTR_{Rex} compared to the solutions without agar (Figure 4). In principle, this limits the inverse approach to applications with pulses that are much shorter or much longer than $1/R_{1\rho}(\Delta\omega)$ The latter corresponds to the cw case. In practice, Z values are directly tunable by B_1 and can be set to values that are not smaller than 0.5; then $R_{1\rho} \sim 2 R_{1a}$ and the condition $R_{1\rho} \cdot t_p \ll 1$ is easier to fulfill.

Pulsed CEST including MT was also studied with similar phantom parameters by Desmond *et al.* (18) who could interpret their data with numerical Bloch-McConnell simulations. By addition of agar T_2 is changed strongly. However, a limitation of our study is that MT was only shown to be corrected up to 1% agar, which corresponds to a fraction of about $f_b = 0.3\%$ (54). In contrast, fractions up to $f_b = 18\%$ are possible in cartilage (55). For cw simulations showed that the inverse superposition is appropriate up to $f_b = 5\%$ (29), but then the assumption of the simple superposition $R_{1\rho} = R_{eff} + R_{ex,CEST} + R_{ex,MT}$ might be invalid.

The intermediate exchange regime was not explicitly considered in this study. In this case the spillover correction of MTR_{Rex} is promising, but has still to be proven. Although demonstrated so far for amine and amide exchange, we expect that our normalization will work for DIACEST and PARACEST in the slow- and intermediate exchange regime, and for the generation of qualitative contrast and quantitative parameter fittings.

Application in the case of non steady-state and inversion pulses

For in-vivo protocols the saturation times are commonly kept shorter, in the range of $1 \cdot T_1 - 2 \cdot T_1$, to save scanning time or avoid dominant spillover effects (6,7). Also, the more efficient inversion pulses are commonly used (23,24,51,53). Additional measurements in non-steady-state with only 3s irradiation ($\sim 1 \times T_1$) were performed (Figure 9abe), as well as saturation with a pulse train of 180° -pulses (Figure 9cdf) for the phantom described in Figure 2. In both cases the homogeneity between the agar phantoms was improved by the inverse evaluation MTR_{Rex} against MTR_{asym} . From theory it is known (32), that the inverse metric is not valid for transient state. However, near steady-state ($t_{\text{sat}} T_1$) it can still be used as an approximation. For inversion transfer or CERT there is no analytical knowledge, but our results indicate that the general Z-spectrum structure might be similar also for rotation transfer.

Systematic and statistical errors

Figure 10 depicts the increase of errors for MTR_{Rex} . If we turn to the $1/Z$ metric the relative errors stay similar $\Delta(1/Z)/(1/Z) = \Delta Z/Z$, but the absolute errors increase: $\Delta(1/Z) = (1/Z^2) \cdot \Delta Z$. For example, $R_1 = 1 \text{ s}^{-1}$ and a dominant direct saturation at the label frequency of $R_{\text{eff}} = 2 \cdot R_1$ leads to $Z = 0.5$. Hence, the statistical error of $1/Z$ is 4 times the error of Z .

However, MTR_{asym} has also a quadratic term of R_{eff} in the denominator, therefore $MTR_{\text{asym}} \sim 1/Z^2 \cdot PTR$. Thus, the CEST effect estimated by MTR_{asym} has a systematic error in the order of $1/Z^2$. This means, by the inverse metric we trade systematic errors against statistical errors, which can be reduced by averaging. This also indicates that B_1 should not exceed a certain limit to keep Z and the SNR large. For the estimation of SNR, MTR_{asym} is a good indicator.

Figure 8 indicates, that a spillover correction is also a B_1 correction near the full-saturation limit ($\alpha \approx 1$). Where MTR_{asym} shows a strong dependence on B_1 and has to be corrected by postprocessing as proposed by Sun *et al.* (47) MTR_{Rex} is nearly constant up to $B_1 = 2 \text{ } \mu\text{T}$. For faster exchange and partial saturation the tissue-dependent B_1 correction of Singh *et al.* (56) reported at $B_0 = 7 \text{ T}$ should be performed with spillover-corrected MTR_{Rex} instead of MTR_{normref} . We do not recommend to apply a B_1 correction on spillover-diluted data, but suggest to apply B_1 corrections to R_{ex} directly.

Imaging of stroke

In the rat CEST imaging study of Sun *et al.* (15) APT of normal tissue was reported to be 2.94% whereas in the lesion it dropped to 0.9%. This was stronger than the signal decrease of about a factor of 0.5 observed in our animal study. Also in pH mapping we only see a drop of 0.5 pH units while a pH-decrease of approx. 1 was reported in ref. (15). In this and other studies (17,39) also the correlation with lesions detected by diffusion and perfusion imaging was investigated. In our experiments resolution was too low to resolve significant substructures within the lesion. In contrast to other studies we avoided contaminations of asymmetry analysis by employing a baseline estimation (45). We think that this is beneficial, especially because significant NOE effects and shifted macromolecular MT effect are apparent in the brain parenchyma. Note that this method can only be applied in higher fields ($B_0 \geq 3 \text{ T}$). For lower B_0 we suggest a Lorentzian-line fit of the water resonance as appropriate reference.

Conclusion

We propose a new spillover- and MT-correction method for evaluation of Z-spectra from CEST experiments which needs no information about T_2 and MT of the system and is easily applied. Validity of the proposed corrected magnetization transfer ratio (MTR_{Rex}) was demonstrated for an *in vitro* system yielding high spillover i.e. creatine in agar gels at clinical field strengths. MTR_{Rex} was extended to a T_1 -relaxation-compensated metric, called AREX for apparent exchange-dependent relaxation, which allowed quantitative evaluation of Z-spectra and could be verified by numerical fits. Validity, sensitivity and performance of the metric require sufficiently large Z-values ($Z > 0.5$) and a proper reference scan. APT-CEST MRI experiments of acute stroke in rat brain at $B_0 = 9.4$ T fulfilled these requirements. The outcome of the evaluation by means of the AREX metric was a significantly higher contrast between stroke area and normal tissue compared to the contrast obtained by use of the non-inverse metric. Hence we propose application of the AREX metric for analysis of Z-spectra data of all pathologies where changes of MT, T_2 , or T_1 are observed, in particular in tumors or tissue affected by stroke. With a proper reference scan AREX may help to provide a pure exchange-dependent and exchange-site-specific contrast.

References

1. Zhou J, Zijl PCM van. Chemical exchange saturation transfer imaging and spectroscopy. *Progress in Nuclear Magnetic Resonance Spectroscopy*. 2006 May;48(2-3):109–36.
2. Van Zijl PCM, Yadav NN. Chemical exchange saturation transfer (CEST): What is in a name and what isn't? *Magn Reson Med*. 2011 Apr;65(4):927–48.
3. Terreno E, Castelli DD, Aime S. Encoding the frequency dependence in MRI contrast media: the emerging class of CEST agents. *Contrast Media Mol Imaging*. 2010 Apr;5(2):78–98.
4. Zhou J, Payen J-F, Wilson DA, Traystman RJ, Zijl PCM van. Using the amide proton signals of intracellular proteins and peptides to detect pH effects in MRI. *Nat Med*. 2003;9(8):1085–90.
5. Haris M, Nanga RPR, Singh A, Cai K, Kogan F, Hariharan H, et al. Exchange rates of creatine kinase metabolites: feasibility of imaging creatine by chemical exchange saturation transfer MRI. *NMR in Biomedicine*. 2012 Nov;25(11):1305–9.
6. Kogan F, Haris M, Singh A, Cai K, Debrosse C, Nanga RPR, et al. Method for high-resolution imaging of creatine in vivo using chemical exchange saturation transfer. *Magn Reson Med*. 2013 Feb 14. doi: 10.1002/mrm.24641
7. Cai K, Haris M, Singh A, Kogan F, Greenberg JH, Hariharan H, et al. Magnetic resonance imaging of glutamate. *Nature Medicine*. 2012 Jan 22;18(2):302–6.
8. Ling W, Regatte RR, Navon G, Jerschow A. Assessment of glycosaminoglycan concentration in vivo by chemical exchange-dependent saturation transfer (gagCEST). *Proc Natl Acad Sci USA*. 2008 Feb 19;105(7):2266–70.
9. Schmitt B, Zbyn S, Stelzeneder D, Jellus V, Paul D, Lauer L, et al. Cartilage quality assessment by using glycosaminoglycan chemical exchange saturation transfer and (^{23}Na) MR imaging at 7 T. *Radiology*. 2011 Jul;260(1):257–64.
10. Singh A, Haris M, Cai K, Kasey VB, Kogan F, Reddy D, et al. Chemical exchange saturation transfer magnetic resonance imaging of human knee cartilage at 3 T and 7 T. *Magn Reson Med*. 2012 Aug;68(2):588–94.

11. Chan K W Y, McMahon M T, Kato Y, Liu G, Bulte J W M, Bhujwala Z M, et al. Natural D-glucose as a biodegradable MRI contrast agent for detecting cancer. *Magn Reson Med*. 2012;68(6):1764–73.
12. Sun P Z, Benner T, Kumar A, Sorensen A G. Investigation of optimizing and translating pH-sensitive pulsed-chemical exchange saturation transfer (CEST) imaging to a 3T clinical scanner. *Magn Reson Med*. 2008 Oct;60(4):834–41.
13. Longo D, Colombo S, Dastrù W, Poggi L, Tedoldi F, Terreno E, et al. CMR2009: 11.02: Evaluating iopamidol as pH-responsive CEST agent at 3 and 7 T. *Contrast Media Mol Imaging*. 2009 Nov;4(6):294–5.
14. Jin T, Wang P, Zong X, Kim S-G. Magnetic resonance imaging of the Amine-Proton EXchange (APEX) dependent contrast. *Neuroimage*. 2012 Jan 16;59(2):1218–27.
15. Sun P Z, Murata Y, Lu J, Wang X, Lo E H, Sorensen A G. Relaxation-compensated fast multislice amide proton transfer (APT) imaging of acute ischemic stroke. *Magn Reson Med*. 2008 May;59(5):1175–82.
16. Sun P Z, Zhou J, Huang J, van Zijl P. Simplified quantitative description of amide proton transfer (APT) imaging during acute ischemia. *Magn Reson Med*. 2007 Feb;57(2):405–10.
17. Sun P Z, Wang E, Cheung J S, Zhang X, Benner T, Sorensen A G. Simulation and optimization of pulsed radio frequency irradiation scheme for chemical exchange saturation transfer (CEST) MRI- demonstration of pH-weighted pulsed-amide proton CEST MRI in an animal model of acute cerebral ischemia. *Magn Reson Med*. 2011 Oct;66(4):1042–8.
18. Desmond K L, Stanisz G J. Understanding quantitative pulsed CEST in the presence of MT. *Magn Reson Med*. 2012 Apr;67(4):979–90.
19. Sun P Z, Sorensen A G. Imaging pH using the chemical exchange saturation transfer (CEST) MRI: Correction of concomitant RF irradiation effects to quantify CEST MRI for chemical exchange rate and pH. *Magn Reson Med*. 2008 Aug;60(2):390–7.
20. Sun P Z, van Zijl P C M, Zhou J. Optimization of the irradiation power in chemical exchange dependent saturation transfer experiments. *Journal of Magnetic Resonance*. 2005 Aug;175(2):193–200.
21. Sun P Z. Simultaneous determination of labile proton concentration and exchange rate utilizing optimal RF power: Radio frequency power (RFP) dependence of chemical exchange saturation transfer (CEST) MRI. *Journal of Magnetic Resonance*. 2010 Feb;202(2):155–61.
22. Zaiss M, Schmitt B, Bachert P. Quantitative separation of CEST effect from magnetization transfer and spillover effects by Lorentzian-line-fit analysis of z-spectra. *Journal of Magnetic Resonance*. 2011 Aug;211(2):149–55.
23. Jones C K, Polders D, Hua J, Zhu H, Hoogduin H J, Zhou J, et al. In vivo three-dimensional whole-brain pulsed steady-state chemical exchange saturation transfer at 7 T. *Magn Reson Med*. 2012 Jun;67(6):1579–89.
24. Dula A N, Arlinghaus L R, Dortch R D, Dewey B E, Whisenant J G, Ayers G D, et al. Amide proton transfer imaging of the breast at 3 T: Establishing reproducibility and possible feasibility assessing chemotherapy response. *Magn Reson Med*. 2013 Jul;70(1):216–24.
25. Lee J-S, Regatte R R, Jerschow A. Isolating chemical exchange saturation transfer contrast from magnetization transfer asymmetry under two-frequency rf irradiation. *Journal of Magnetic Resonance*. 2012 Feb;215(0):56–63.

26. Scheidegger R, Vinogradov E, Alsop DC. Amide proton transfer imaging with improved robustness to magnetic field inhomogeneity and magnetization transfer asymmetry using Saturation with Frequency Alternating RF Irradiation (SAFARI). *Magn Reson Med*. 2011 Nov;66(5):1275–85.
27. Zu Z, Janve VA, Li K, Does MD, Gore JC, Gochberg DF. Multi-angle ratiometric approach to measure chemical exchange in amide proton transfer imaging. *Magn Reson Med*. 2012 Sep;68(3):711–9.
28. Zu Z, Janve VA, Xu J, Does MD, Gore JC, Gochberg DF. A new method for detecting exchanging amide protons using chemical exchange rotation transfer. *Magn Reson Med*. 2013 Mar 1;69(3):637–47.
29. Zaiss M, Bachert P. Equivalence of spin-lock and magnetization transfer NMR experiments. arXiv:12032067 [Internet]. 2012 Mar 9; Available from: <http://arxiv.org/abs/1203.2067>
30. Santyr GE, Fairbanks EJ, Kelcz F, Sorenson JA. Off-resonance spin locking for MR imaging. *Magnetic Resonance in Medicine*. 1994 Jul;32(1):43–51.
31. Zaiss M, Schnurr M, Bachert P. Analytical solution for the depolarization of hyperpolarized nuclei by chemical exchange saturation transfer between free and encapsulated xenon (HyperCEST). *The Journal of Chemical Physics*. 2012;136(14):144106.
32. Zaiss M, Bachert P. Exchange-dependent relaxation in the rotating frame for slow and intermediate exchange – modeling off-resonant spin-lock and chemical exchange saturation transfer. *NMR in Biomedicine*. 2013 May; 26(5):507-518
33. Woessner DE, Zhang S, Merritt ME, Sherry AD. Numerical solution of the Bloch equations provides insights into the optimum design of PARACEST agents for MRI. *Magnetic Resonance in Medicine: Official Journal of the Society of Magnetic Resonance in Medicine / Society of Magnetic Resonance in Medicine*. 2005 Apr;53(4):790–9.
34. Trott O, Palmer AG 3rd. Theoretical study of R(1rho) rotating-frame and R2 free-precession relaxation in the presence of n-site chemical exchange. *J Magn Reson*. 2004 Sep;170(1):104–12.
35. Liu G, Gilad AA, Bulte JWM, van Zijl PCM, McMahon MT. High-throughput screening of chemical exchange saturation transfer MR contrast agents. *Contrast Media Mol Imaging*. 2010 May;5(3):162–70.
36. Liu G, Song X, Chan KWY, McMahon MT. Nuts and bolts of chemical exchange saturation transfer MRI. *NMR Biomed*. 2013 Jan 10; doi: 10.1002/nbm.2899
37. Zhou J, Wilson DA, Sun PZ, Klaus JA, Zijl PCMV. Quantitative description of proton exchange processes between water and endogenous and exogenous agents for WEX, CEST, and APT experiments. *Magnetic Resonance in Medicine: Official Journal of the Society of Magnetic Resonance in Medicine / Society of Magnetic Resonance in Medicine*. 2004 May;51(5):945–52.
38. Zhou J, Payen J-F, Wilson DA, Traystman RJ, Zijl PCM van. Using the amide proton signals of intracellular proteins and peptides to detect pH effects in MRI. *Nat Med*. 2003;9(8):1085–90.
39. Sun PZ, Wang E, Cheung JS. Imaging acute ischemic tissue acidosis with pH-sensitive endogenous amide proton transfer (APT) MRI—Correction of tissue relaxation and concomitant RF irradiation effects toward mapping quantitative cerebral tissue pH. *NeuroImage*. 2012 Mar;60(1):1–6.
40. Goerke S, Zaiss M, Bachert P. Water Exchange (WEX) Spectroscopy on creatine model solutions. *Proceedings 29th Annual Scientific Meeting ESMRMB*. Lisbon, Portugal; 2012. p. 394.
41. McMahon MT, Gilad AA, Zhou J, Sun PZ, Bulte JWM, van Zijl PCM. Quantifying exchange rates in chemical exchange saturation transfer agents using the saturation time and saturation power dependencies of the magnetization transfer effect on the magnetic resonance imaging signal (QUEST

- and QUESP): Ph calibration for poly-L-lysine and a starburst dendrimer. *Magn Reson Med.* 2006 Apr;55(4):836–47.
42. Kim M, Gillen J, Landman BA, Zhou J, Zijl PCM van. Water saturation shift referencing (WASSR) for chemical exchange saturation transfer (CEST) experiments. *Magnetic Resonance in Medicine.* 2009 Jun;61(6):1441–50.
 43. Liu K, Mori S, Takahashi HK, Tomono Y, Wake H, Kanke T, et al. Anti-high mobility group box 1 monoclonal antibody ameliorates brain infarction induced by transient ischemia in rats. *FASEB J.* 2007 Dec;21(14):3904–16.
 44. Hu X, Le TH. Artifact reduction in EPI with phase-encoded reference scan. *Magn Reson Med.* 1996 Jul;36(1):166–71.
 45. Jin T, Wang P, Zong X, Kim S-G. MR imaging of the amide-proton transfer effect and the pH-insensitive nuclear overhauser effect at 9.4 T. *Magn Reson Med.* 2013 Mar 1;69(3):760–70.
 46. Roeloffs V, Zaiss M, Bachert P. An analytical approach towards pulsed-SL/CEST quantification. *Proceedings of 21st Annual Meeting of ISMRM.* Salt Lake City; 2013. p. 2546.
 47. Sun PZ, Farrar CT, Sorensen AG. Correction for artifacts induced by B(0) and B(1) field inhomogeneities in pH-sensitive chemical exchange saturation transfer (CEST) imaging. *Magnetic Resonance in Medicine.* 2007 Dec;58(6):1207–15.
 48. Trott O, Palmer AG 3rd. Theoretical study of R(1rho) rotating-frame and R2 free-precession relaxation in the presence of n-site chemical exchange. *J Magn Reson.* 2004 Sep;170(1):104–12.
 49. Haris M, Nath K, Cai K, Singh A, Crescenzi R, Kogan F, et al. Imaging of glutamate neurotransmitter alterations in Alzheimer's disease. *NMR in Biomed.* 2012 doi:10.1002/nbm.2875
 50. Saar G, Zhang B, Ling W, Regatte RR, Navon G, Jerschow A. Assessment of glycosaminoglycan concentration changes in the intervertebral disc via chemical exchange saturation transfer. *NMR Biomed.* 2012 Feb;25(2):255–61.
 51. Zu Z, Li K, Janve VA, Does MD, Gochberg DF. Optimizing pulsed-chemical exchange saturation transfer imaging sequences. *Magn Reson Med.* 2011 Oct;66(4):1100–8.
 52. Tee YK, Khrapitchev AA, Sibson NR, Payne SJ, Chappell MA. Evaluating the use of a continuous approximation for model-based quantification of pulsed chemical exchange saturation transfer (CEST). *J Magn Reson.* 2012 Sep;222:88–95.
 53. Jones CK, Huang A, Xu J, Edden RAE, Schär M, Hua J, et al. Nuclear Overhauser enhancement (NOE) imaging in the human brain at 7 T. *NeuroImage.* 2013 Aug 15;77:114–24.
 54. Henkelman RM, Huang X, Xiang QS, Stanisz GJ, Swanson SD, Bronskill MJ. Quantitative interpretation of magnetization transfer. *Magn Reson Med.* 1993 Jun;29(6):759–66.
 55. Stanisz GJ, Odobina EE, Pun J, Escaravage M, Graham SJ, Bronskill MJ, et al. T1, T2 relaxation and magnetization transfer in tissue at 3T. *Magnetic Resonance in Medicine.* 2005;54(3):507–12.
 56. Singh A, Cai K, Haris M, Hariharan H, Reddy R. On B(1) inhomogeneity correction of in vivo human brain glutamate chemical exchange saturation transfer contrast at 7T. 2013 Mar 1;69(3):818-24

Figure Captions

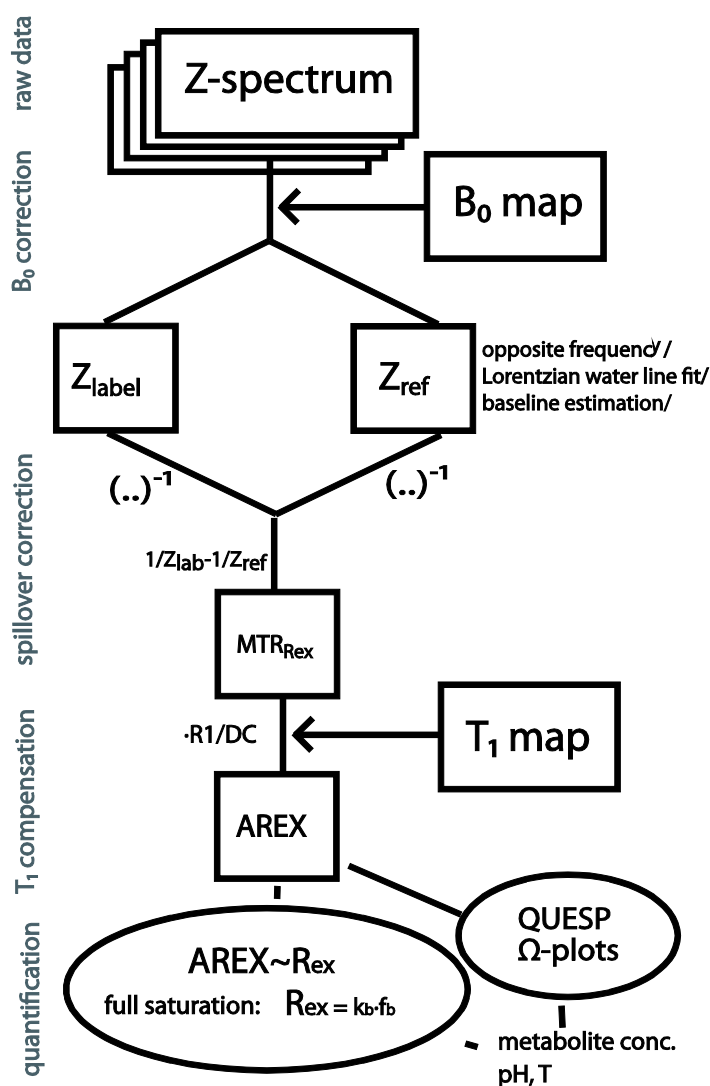


Figure 1

: Scheme of data evaluation for spillover- and T_1 -compensated CEST. Only simple matrix operations are performed to get the AREX contrast. The step of defining a suitable reference value Z_{ref} is crucial.

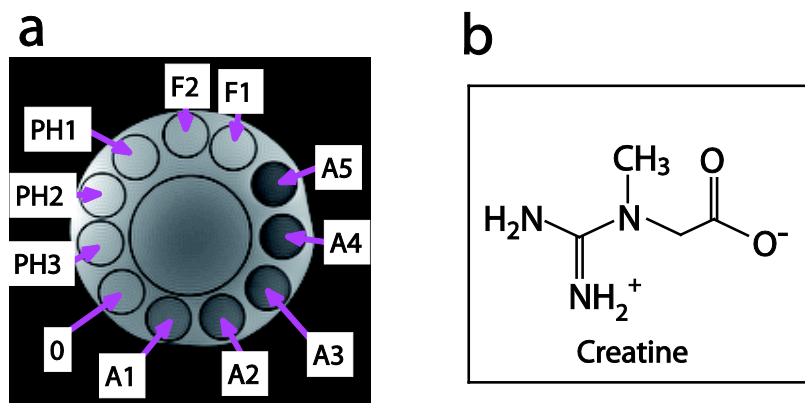


Figure 2

: a) Turbo-spinecho (TSE) image of the employed phantom (for details see Table 1). #0 is the reference solution with 55.5 mM creatine and PBS at pH = 6.38 and without agar. The #Ax phantoms differ from #0 by increasing agar concentration (0.2% – 1%). The #PHx phantoms differ from #0 by altered pH (6.2, 6.3, 6.6). The #Fx phantoms have different creatine concentrations compared to #0 (#F1: 55.5 mM 1/3, #F2: 55.5 mM 2/3). (b) zwitterionic form of aqueous creatine occurring at low pH.

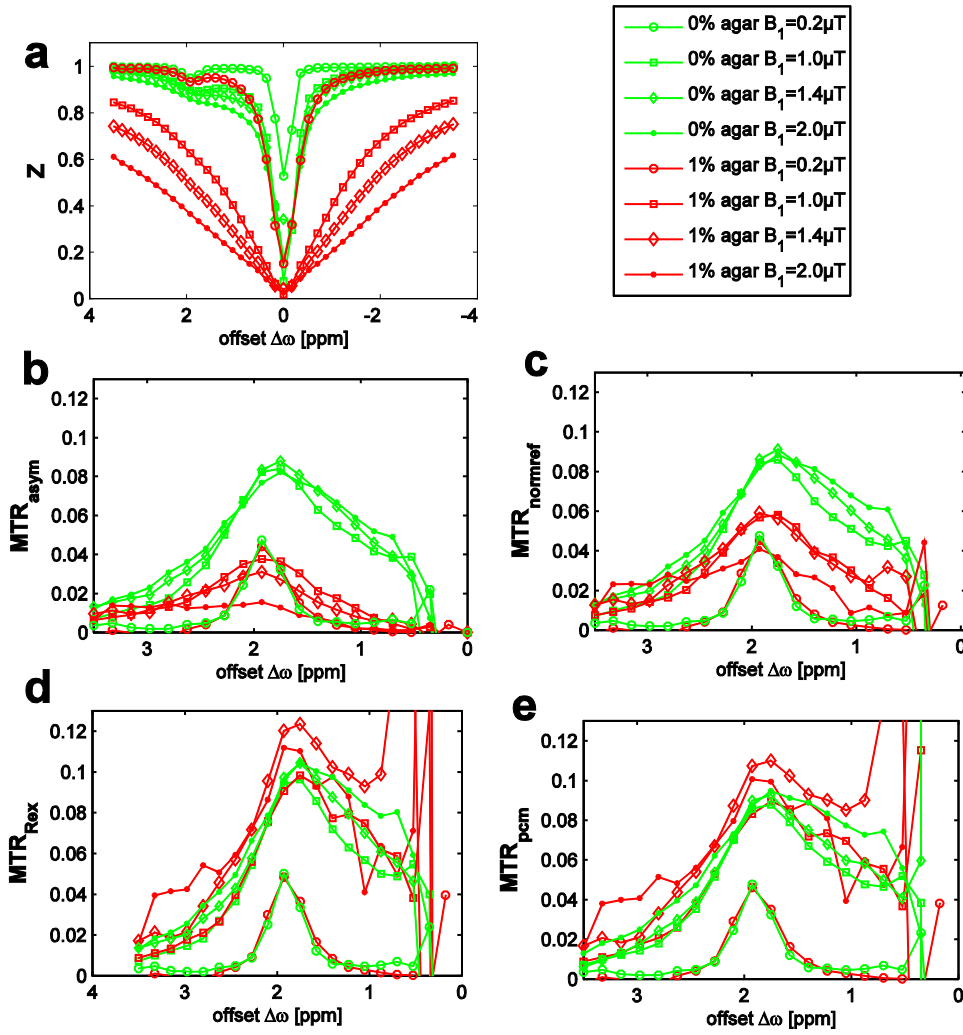


Figure 3

(a) Z-spectra obtained with different B_1 from creatine solutions with 1% agar (blue lines, #A5) and 0% agar (red lines, #0). The labeling increases with B_1 , but also the direct saturation effect: for low B_1 of $0.2 \mu\text{T}$ (circles) the spillover effect is negligible (a) which explains why curves overlap for all metrics (b–e). (b) MTR_{asym} shows the strong spillover dilution in the solidified phantom (with agar) whereas MTR_{Rex} (d) and MTR_{pcm} (e) are able to correct the dilution so that aqueous and solidified phantoms yield almost the same effect. The spillover correction proposed by Liu *et al.* (c) (eq. (8) in Ref.(35)) compensates spillover partially. Error bars are omitted for better visibility; they increase strongly for higher spillover correction as depicted in Figure 10.

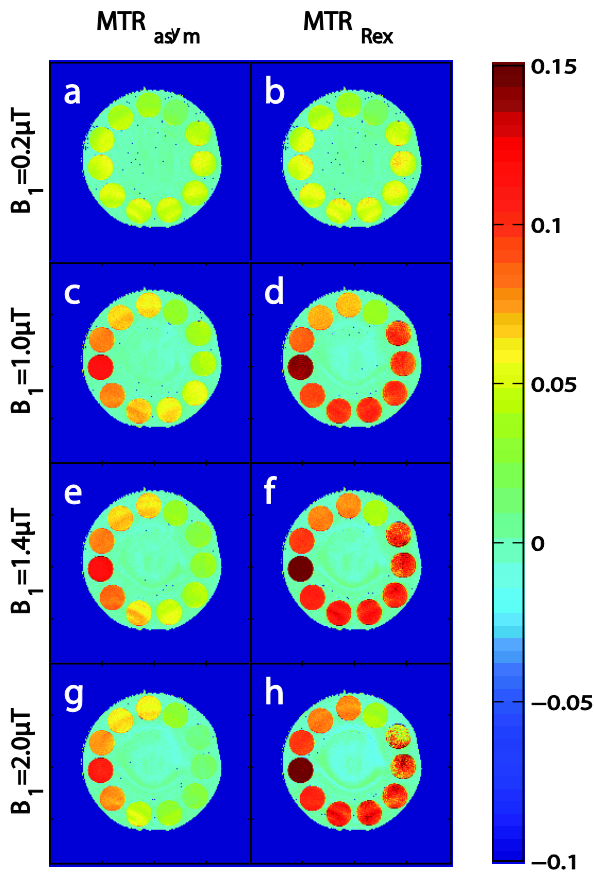


Figure 4

Comparison of the normalizations MTR_{asym} (left column) and MTR_{Rex} (right column) for $B_1 = 0.2, 1.0, 1.4,$ and $2.0 \mu\text{T}$. In each case the estimation of the CEST effect is higher for MTR_{Rex} . The phantoms with varying agar concentration (#0, #A1–#A5) show similar contrast in MTR_{Rex} , whereas MTR_{asym} shows diluted contrast with increasing agar concentration. Differences in pH and creatine concentration are reflected in both MTRs. Therefore, MTR_{Rex} has all properties of a spillover correction.

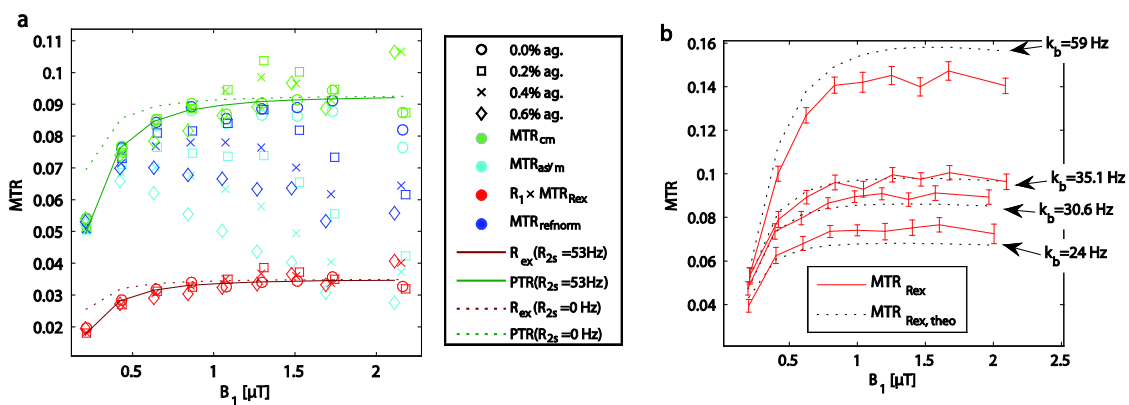


Figure 5

(a) ROI evaluation of ROIs #0 and #A1–#A3 with the proposed spillover corrections. For all agar concentrations and B_1 values, both MTR_{pcm} (green) and MTR_{Rex} (red) appear to be in a narrow band around the control without agar #0. MTR_{asym} (cyan) and MTR_{normref} (blue) show a much stronger decrease with increasing B_1 and agar. (b) MTR_{Rex} from data and from theory (eq. (15)) employing parameters of the numerical fit (Table 1): The curves match roughly and the dependence on k_b and B_1 is very similar.

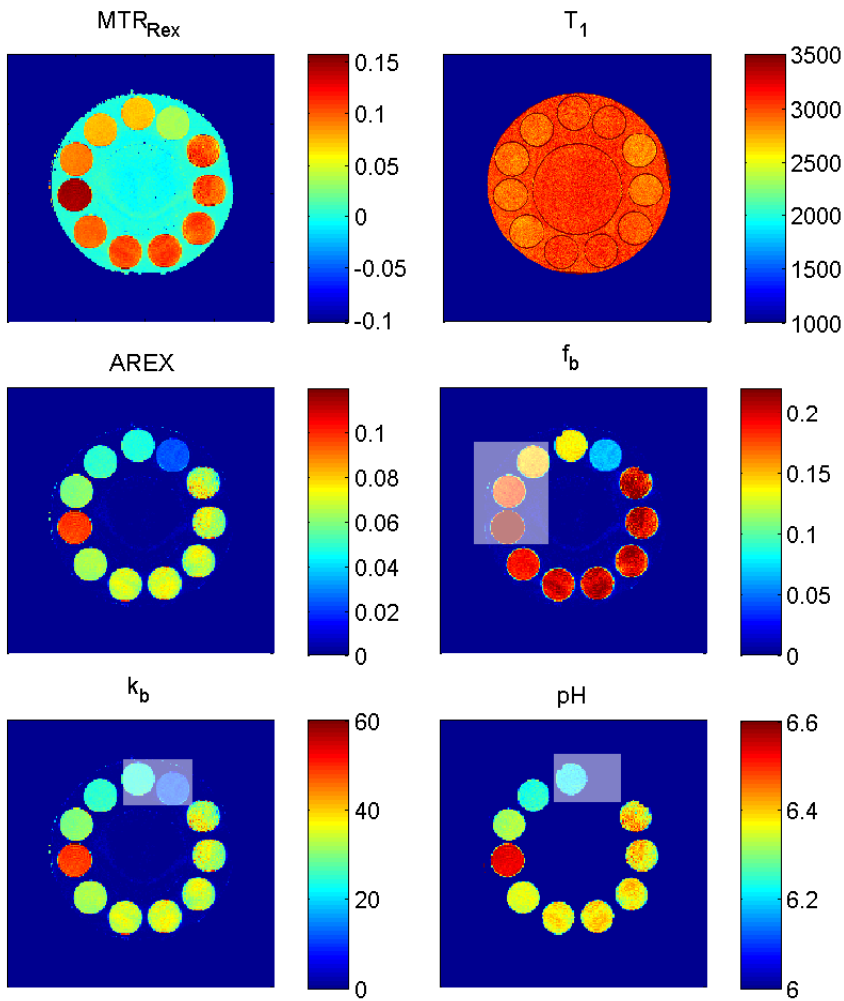


Figure 6

Quantitative pulsed CEST-MRI. (a) MTR_{Rex} evaluated for $B_1 = 1 \mu\text{T}$. Employing the T_1 map (b) the spillover-corrected and T_1 -compensated ARES map can be calculated. Under the assumption of full saturation ARES yields a k_a -map. (c) f_b -map employing the exchange rate for creatine $k(\text{pH} = 6.38, T = 19^\circ\text{C}) = 35 \text{ s}^{-1}$; it suggests that creatine has 4 exchanging protons. Using $f_b = 0.2\%$ a k_b -map (e) can be obtained from ARES which correlates well with results from WEX measurements. (f) Therefore, a $\text{pH}(k_b)$ -map can be obtained using Eq. (16). Gray boxes indicate tubes where concentration or pH was not constant.

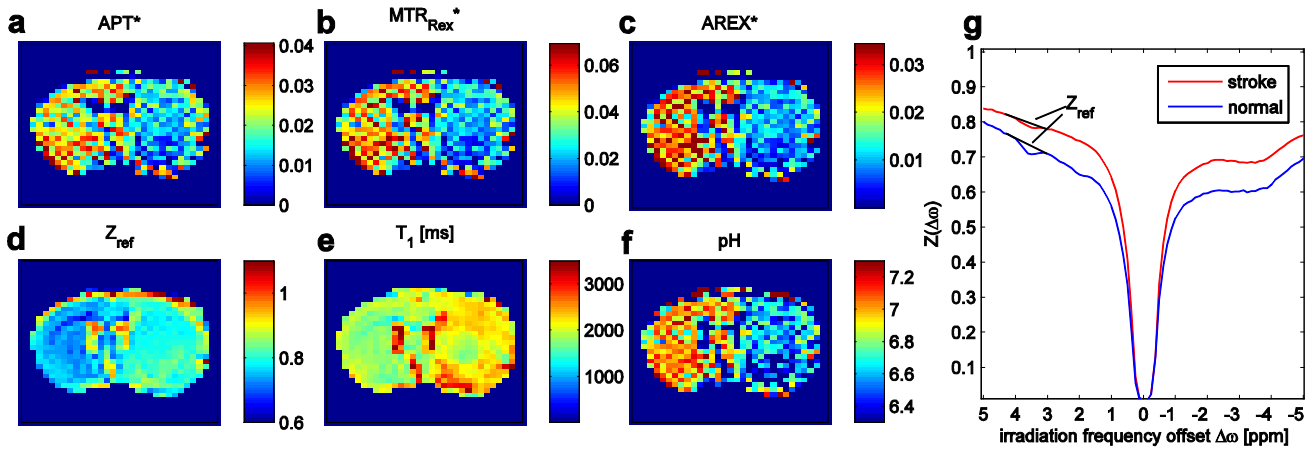


Figure 7

: Amide proton transfer (APT) contrast obtained by pulsed CEST-MRI of rat with acute stroke. APT contrast (a) is contaminated by T_1 (e) and spillover effects (visible in the reference image (d)). After correction of spillover by the inverse metric MTR_{Rex} the contrast between lesion and normal tissue increases (b). The T_1 -corrected AREX evaluation yields a pure exchange-weighted contrast which shows even higher signal drop in the stroke lesion compared to normal tissue. (e) From AREX an absolute pH map can easily be obtained by eq. (19). For all CEST maps the average of Z-values at 4.2 and 3 ppm was employed as a reference (eq. 21) as illustrated by the baselines in the Z-spectra in (g). To achieve good visual comparison of the contrast each MTR map was windowed from zero to two times the average value of all non-zero pixels. CEST-EPI parameters were: matrix size = 64, echo time = 28 ms. Pulse train parameters were $t_p = 12.5$ ms, $B_1 = 0.84$ μ T, DC = 50%, flip angle = 180° , $n = 200$.

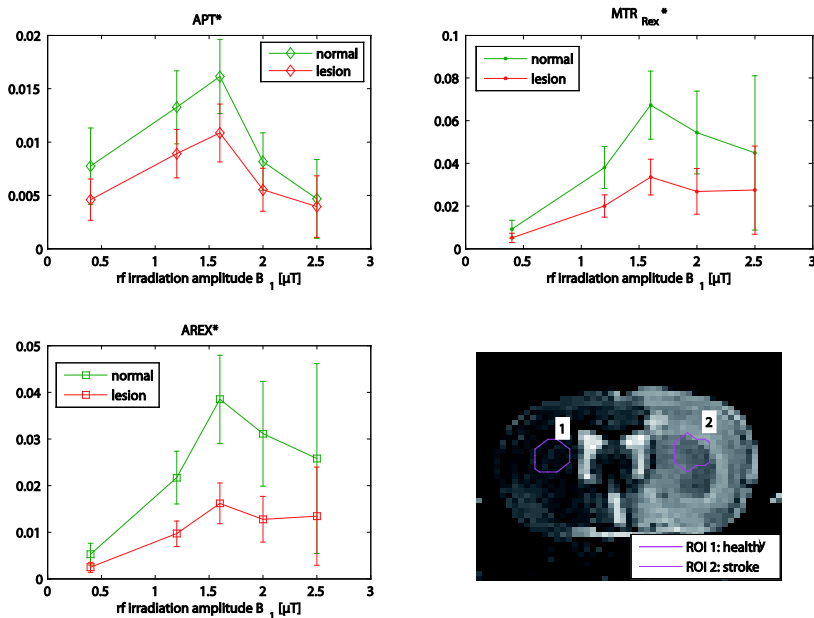


Figure 8

: ROI-evaluation of the three-point methods APT*, the spillover-corrected MTR_{Rex}, and spillover- and T₁-compensated AREX. Similar to the phantom study APT* shows a strong decrease with B₁ for values higher than 1.5 uT, whereas MTR_{Rex} and AREX show less decrease of signal for higher B₁. This pattern is similar to the phantom results (compare Figure 5) and indicates validity of the spillover correction. However, the plateau of full-saturation limit is not reached, caused by probably by contaminations of the reference scan. Important to note is that the difference between signals in the stroke lesion and normal tissue are much more significant after spillover correction and T₁ compensation. Under assumption of equal amide concentrations in stroke and normal tissue, the signal drop reflects a change in exchange rate of about a factor of two.

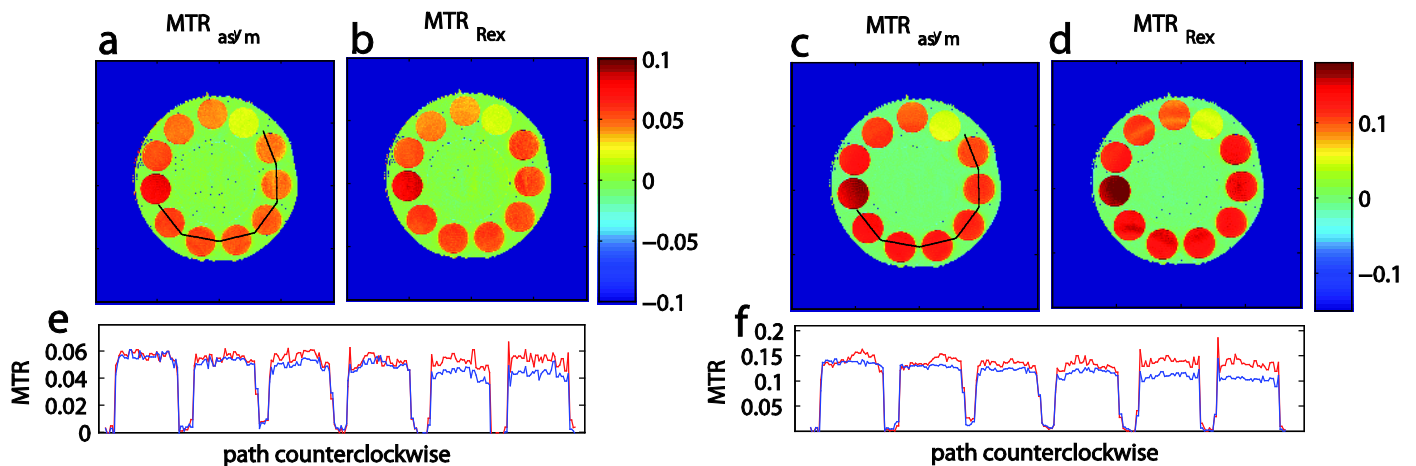


Figure 9:

MTR_{asym} (a,c) and the inverse approach MTR_{Rex} (b,d) for the practical relevant cases of (a,b) non-steady state saturation ($t_{sat}=3.1$ s, $B_1 = 0.5$ μT, $t_p = 100$ ms, DC=50%, $n = 16$) and (b,d) 180° pulsed saturation (180°-pulses: $B_1 = 0.48$ μT, $t_p = 25$ ms, DC=50% $n = 320$). Profiles along the path (counterclockwise) defined in (a) show that MTR_{Rex} (red line) corrects the decrease of MTR_{asym} (blue line) with increasing agar concentration.

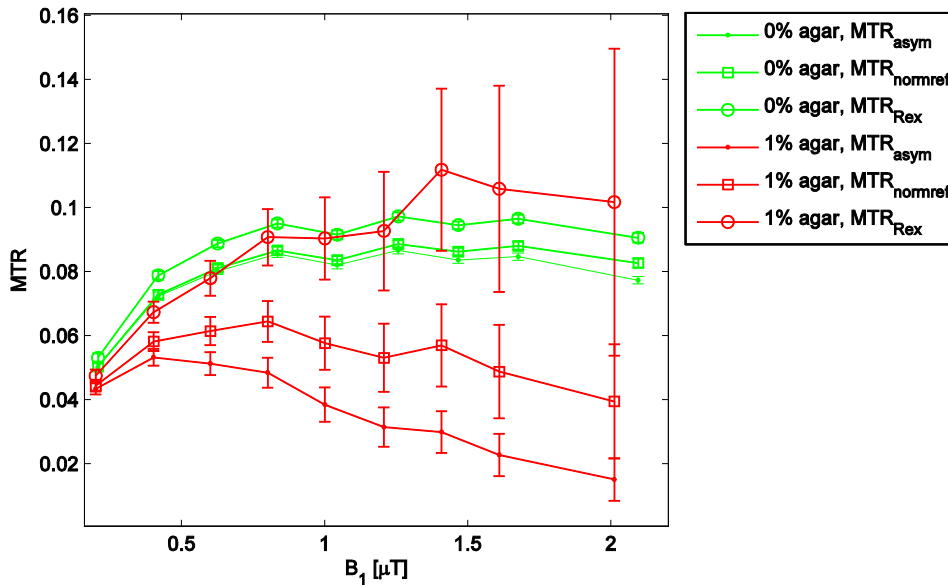
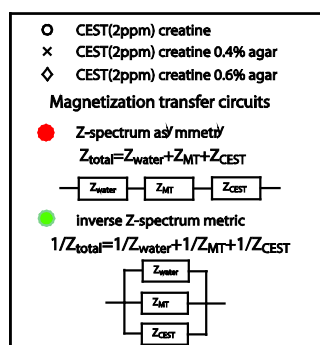
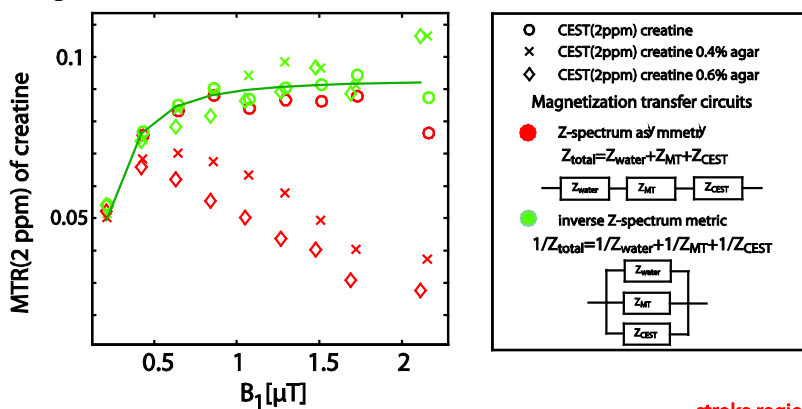


Figure 10

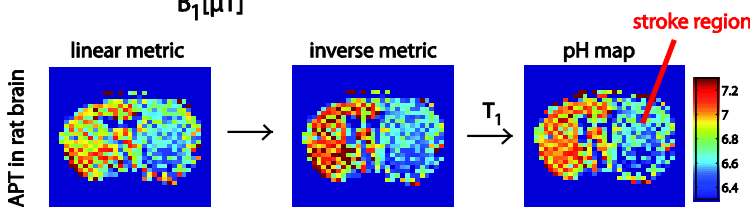
: Error estimation of inverse metric. Absolute errors increase with increasing spillover effect. This results from the error propagation of the inverse metric. However, relative errors do not change and therefore contrast-to-noise ratio is not affected. The systematic spillover deviation is traded with a statistical fluctuation. Original errors were scaled by a factor of one third to improve visibility.

Graphical abstract



Inverse Z-spectrum analysis for MT- and spillover-corrected and T1-compensated steady-state pulsed CEST-MRI – application to pH-weighted MRI of acute stroke

The different effects that influence the Z-spectrum behave like resistors in a parallel circuit and not in a serial circuit. The spillover effect can thus be removed by using the inverse metric MTR_{Rex} . MTR_{Rex} yields the exchange dependent relaxation and allows clean CEST effect evaluation which is applied to spillover- and MT-corrected and T₁-compensated pH-weighted amide proton transfer imaging of acute stroke.



M.Zaiss, J.Xu, S.Goerke,
 I.S.Khan, R.J.Singer, J.C.Gore,
 D.F.Gochberg, P.Bachert